Iranian Journal of Science & Technology, Transaction A, Vol. 29, No. A1
Printed in The Islamic Republic of Iran, 2005

GEOTHERMOBAROMETRY OF Al_2SiO_5-BEARING METAPELITES IN THE ARDARA AUREOLE, NW IRELAND: AN IMPLICATION FOR P-T STABILITY FIELD OF ALUMINIUM SILICATE POLYMORPHS*

S. M. HOMAM**

Faculty of Earth Sciences, Damghan University of Sciences, Cheshmeh-Ali Road, Damghan, I. R. of Iran, Email: m_homam@dubs.ac.ir

Abstract – Andalusite, kyanite and sillimanite occur in well-defined zones in the Ardara aureole, NW Ireland. Temperature and pressure conditions of the Al_2SiO_5-bearing pelites in this aureole were estimated using ten different calibrations of garnet-biotite thermometry and five calibrations of garnet-plagioclase-Al_2SiO_5-quartz barometry. The different calibrations provide different estimates of temperature and pressure. However, using the most recent, and the best reversed experimental data give temperatures varying from 510 to 605 ºC, and a pressure of around 4 kbar across the Ardara aureole. The calculated temperatures for the analyzed samples are compared with published andalusite=sillimanite equilibria, and these equilibria are evaluated in the Ardara aureole.

Keywords – Aluminium silicate polymorphs, geothermobarometry, metapelite, aureole, ardara

1. INTRODUCTION

Andalusite, sillimanite and kyanite are polymorphs of the compound Al_2SiO_5. The wide occurrence of the aluminium silicate polymorphs in metapelites, coupled with the apparently simple pressure-temperature phase equilibrium relations, make the study of this system very attractive to metamorphic petrologists and experimentalists [1]. However, considerable uncertainty shrouds the calibration of P-T phase equilibria involving these phases [1]. This problem is exemplified by the old, but still true, statement of Holdaway [2]: "The Al_2SiO_5 phase diagram is perhaps the most studied and least well defined silicate phase diagram."

Contact aureoles provide a simpler situation to study the factors involved in the development of aluminium silicate polymorphs than regional metamorphism as they occur essentially under isobaric conditions, and typically have far simpler thermal and tectonic histories than regional metamorphism. In a review by Pattison and Tracy [3], of 68 contact aureoles, only 4 aureoles are reported to contain coexisting all aluminium silicate polymorphs formed during a single metamorphic event. Andalusite, kyanite and sillimanite (prismatic and fibrous) are present in the Ardara aureole, thus the estimation of the temperature and pressure conditions of the Al_2SiO_5-bearing pelites in this aureole provide an excellent situation to study the P-T stability field of the aluminium silicate polymorphs.

*Received by the editor December 15, 2003 and in final revised form January 23, 2005
**Corresponding author

2. GEOLOGICAL SETTING

The Donegal region is located in the north west of the Republic of Ireland. The geology of the Donegal region has been comprehensively reviewed by Pitcher and Berger [4]. The country rocks of Donegal granites consist of Dalradian metasedimentary and meta-igneous rocks that range in age from the Late Precambrian to Middle Cambrian age. This group of rocks subsequently underwent major deformation (the Caledonian orogeny) during late Cambrian to late Ordovician eras. The granites of Donegal have been divided into six units having different ages, composition and modes of emplacement.

The Ardara pluton, which is the southernmost of the Donegal granites, has a tear-drop shape and is about 8 kilometres in diameter. It consists of two units, an outer ring of quartz-monzodiorite and an inner core, with the composition varying from quartz-monzodiorite to granodiorite.

The northern Ardara aureole, which is the focus of the present study, consists of a pelitic horizon and an adjacent limestone unit. The pelitic horizon of the northern Ardara aureole consists of interlayered aluminous pelites and semipelites. Lenses and pods of metadolerite are also common in a zone extending about 200 metres from the contact with the Ardara pluton [5]. The Ardara aureole represents a forcibly emplaced, diapiric intrusion [6].

The contact metamorphism of the Ardara pluton has been studied in detail by many previous works [5, 7-9]. In brief, the metamorphic effects of the Ardara pluton extend nearly 1.5 km from the intrusion contact. The rocks of the aureole show a strong foliation. The regional structures, S_1, S_2-S_3, are steepened and intensified in the aureole [4]. The steepening of regional structures can be seen from 800 metres to 1 kilometre from the contact [10]. Akaad [5, 6], Pitcher and Berger [4] and Holder [11] attributed the squeezing and reinforcing of regional structures in the contact aureole to the emplacement of the granite pluton. However, Vernon and Paterson [10] suggested the possibility of syn- or post-emplacement regional deformation.

The Ardara aureole has been divided into two units [6]:

1) an outer unit which is made up of the non-porphyroblastic rocks showing minor contact effects and characterised by new thermal biotite flakes crosscutting the regional schistosity;

2) an inner unit which comprises three zones [8] (Fig. 1) on the basis of prismatic Al_2SiO_5 polymorphs found;

an outer kyanite-bearing andalusite zone,

a middle kyanite-free andalusite zone,

an inner prismatic sillimanite zone.

Naggar and Atherton [8] demonstrated that kyanite in the Ardara aureole is restricted to rocks with MgO/(MgO+FeO) values higher than 0.50, and lower bulk-rock MgO/(MgO+FeO) ratios precluded kyanite as a phase in the assemblage.

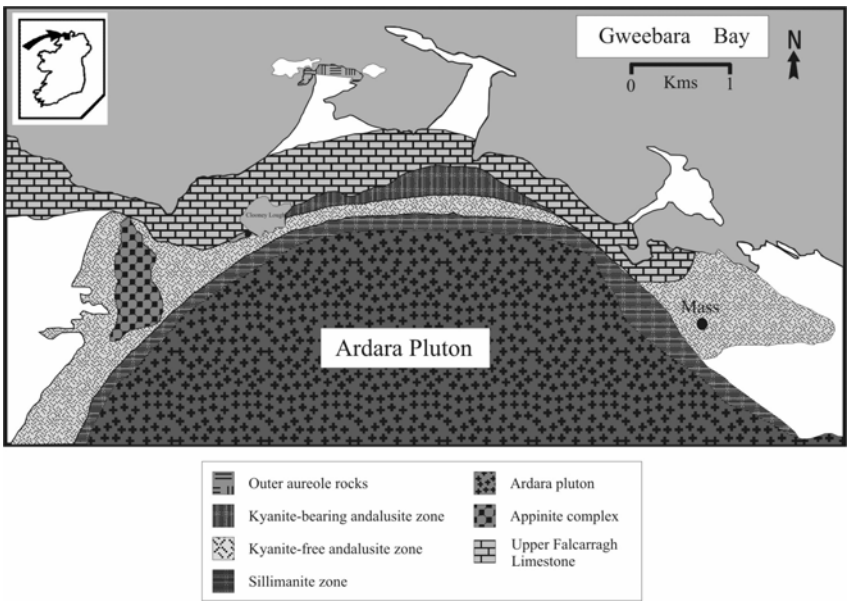

Fig. 1. Geology of the northern portion of the Ardara pluton and surrounding country (modified from Akaad, [6] and [8])

3. PETROGRAPHY OF THE METAPELITIC ROCKS FROM THE ARDARA AUREOLE

The details of textural and mineralogical characteristics of aluminium silicate-bearing rocks from the contact aureole of the Ardara pluton are given elsewhere [9]. In brief, dark porphyroblastic schists with conspicuous andalusite on most surfaces characterise the outer kyanite-bearing andalusite zone. In a thin section, typical rocks consist of quartz + plagioclase + biotite + muscovite ± chlorite ± staurolite ± garnet ± kyanite ± andalusite ± fibrolite. Graphite and ilmenite are also present. Kyanite takes place as small idioblastic to subidioblastic prisms (0.15-0.35 mm in length). Crosscut by kyanite, biotite is usually not disturbed along the kyanite boundaries. Idioblastic kyanite occurs as inclusions within andalusite porphyroblasts. Kyanite is also found included in plagioclase poikiloblasts. Staurolite commonly takes place as small (0.12-0.35 mm in diameter) subidioblastic generally inclusion-free grains. In some slides staurolite can be seen as irregular grains, or clusters of grains, disseminated throughout the rock. Staurolite is also found as relatively large porphyroblasts (0.4-0.9 mm in diameter) containing continuous curved trails of quartz inclusions. Staurolite, with good crystal faces, is commonly included in andalusite and plagioclase porphyroblasts. Garnet occurs only in kyanite-free rocks i.e., kyanite and garnet never occur together in the same rock. It develops as tiny (0.09-0.13 mm in diameter) idioblastic crystals in the groundmass. It also occurs as inclusions in andalusite, plagioclase and staurolite, suggesting garnet was formed earlier than these minerals. Andalusite comes as large porphyroblasts (1-5 mm in diameter) and include quartz, staurolite, kyanite, garnet and ore minerals. Fibrolite occurs as bundles dominantly decolouring and replacing biotite. Anastomosing is found around plagioclase porphyroblasts. Fibrolite also occurs as discontinuous folia anastomosing between lenticular grains of quartz in the groundmass. In some instances it appears that andalusite encloses fibrolite or parts of the fibrolitised biotite. Plagioclase always takes place as porphyroblasts (0.5-4 mm in diameter). It generally shows "S"-shaped inclusion trails of quartz. The textures exhibited by plagioclase could easily be mistaken as textures evolving

from rotated porphyroblasts. However, these textures are clearly formed by overprinting regional microfolds (S_2-S_3) in the groundmass.

Within the kyanite-free andalusite schists, andalusite can be seen to consist of an inclusion-free pink pleochroic core with the mantle of colourless poikilitic andalusite. A common feature in idioblastic andalusites is the development of textural sector-zoning and matrix displacement. Other common minerals are garnet, staurolite and fibrolite. Staurolite and garnet display similar textural features to those in the kyanite-bearing andalusite zone. In many examples fibrolite folia are concentrated in narrow high strain zones between andalusite porphyroblasts where the presence of tight crenulations in the fibrolite folia is evident. Fibrolite is also found anastomosing around andalusite porphyroblasts. This textural evidence suggests syn-deformational growth of fibrolite [12].

The inner sillimanite zone is characterised by dark brown hornfelses with biotite, garnet and occasionally sillimanite visible in hand specimens. Under the microscope, the overall textures of the rock suggest that the transformation from the kyanite-free andalusite zone to the sillimanite zone was accompanied by a wholesale textural reconstitution [13]. Sillimanite appears as long prisms growing from the groundmass as well as large grains to show symplectic intergrowth with quartz in the groundmass. In some of the specimens, sillimanite is formed by the coarsening of fibrolite groundmass. In one slide, square areas about 4 millimetres in diameter may be presumed from the resemblance of the morphology to be andalusite, pseudomorphed by sillimanite. Fibrolite is commonly concentrated in folia that anastomose between pods rich in biotite, quartz and plagioclase. Staurolite occurs as tiny subhedral grains throughout the groundmass. Garnet in most of the samples from the sillimanite zone displays two different habits. Away from the contact it occurs as small idioblastic to subhedral crystals in biotite clusters after regional garnet. At the immediate contact with the pluton, garnet is present as large porphyroblasts (1-1.5 mm in diameter) which contain inclusions of biotite, quartz and fibrolite. Cordierite can be seen as xenoblastic grains throughout the groundmass. It also occurs as large porphyroblasts (4-8 mm in diameter) which contain inclusions of fibrolite and biotite.

4. GEOTHERMOBAROMETRY IN METAPELITIC ROCKS FROM THE ARDARA AUREOLE

Several geothermobarometers have been used for the estimation of temperature and/or pressure in metapelites, e.g. garnet-biotite; garnet-chlorite; garnet-cordierite thermometers and garnet-plagioclase-Al_2SiO_5-quartz, garnet-plagioclase-muscovite-biotite and garnet-plagioclase-muscovite-quartz barometers. However, it appears that the garnet-biotite thermometer and garnet-plagioclase-Al_2SiO_5-quartz barometer are the most widely used geothermobarometers in metapelites of low to intermediate grade [14]. Fortunately garnet is present in many samples throughout the Ardara aureole, accompanied by Al_2SiO_5, and thus provides an excellent situation to employ garnet-biotite thermometry and garnet-plagioclase-Al_2SiO_5-quartz barometry.

In this study eight pelitic samples were collected for geothermobarometry estimates from rocks lying in the inner sillimanite zone (82, 81, 76 and 73), the middle kyanite-free andalusite zone (53, 48 and 36) and the outer kyanite-bearing andalusite zone (7) (Fig. 2). The samples were chosen as they contained the required phases (garnet, Al_2SiO_5, biotite and plagioclase) and are least affected by retrograde alteration.

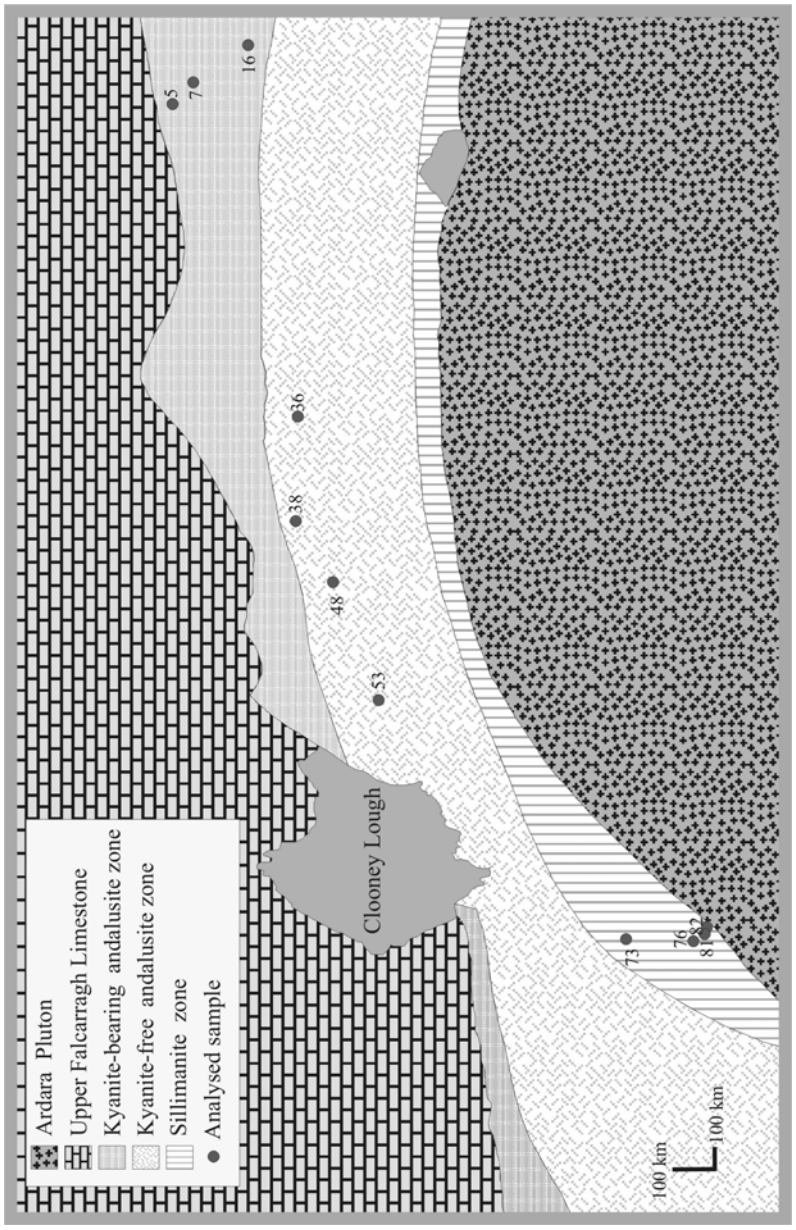

Fig. 2. Sample localities in the inner aureole of the Ardara pluton showing analysed rocks for mineral chemistry and geothermobarometry, Zonal arrangement determined on basis of aluminum silicate polymorphs distribution

Compositions of minerals in a polished thin section were analysed with an automated electron-microprobe analyser at the University of Liverpool. Mineral data were acquired on a Philips XL-30 Scanning Electron Microscope. The operating condition was15-20 kV Electron beam accelerating voltage. Microprobe X-ray analyses were produced with the Oxford ISIS Series 300 Microanalysis System. Data reduction followed the Bence-Albee scheme using α factors computed according to the procedure of Albee and Ray [15].

Garnet, biotite and plagioclase were analysed for geothermometry and geobarometry. Biotite is chemically homogenous. Strongly zoned garnets were present in four samples (samples 76, 73, 48 and 7) i.e., normal zoning with decreasing Mn and Ca and increasing Mg and Fe towards the rim of

the crystal (Fig. 3). However, small marginal discrepancies do occur. Such marginal discrepancies indicate reversed zoning in which MnO shows an increase, whereas MgO shows a decrease towards the garnet edge (Fig. 3). This feature is most likely due to late retrograde re-equilibrium between the outer rim of garnet and rock groundmass. Garnets from the four remaining samples are unzoned (samples 82, 81, 53 and 36).

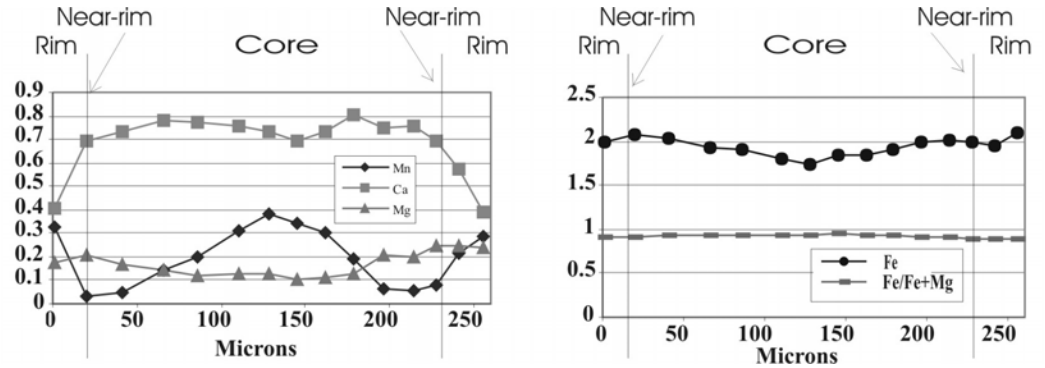

Fig. 3. Chemical zonation in garnet (sample 7) from the Ardara aureole

Most garnets in metapelites of the Ardara aureole display varying degrees of developing atoll forms [16]. In the garnet-biotite geothermometry, euhedral garnet analyses coupled with matrix biotite composition were used. The reason for the choice of euhedral garnet rather than those with atoll form is that the chemistry and zoning profile of garnet are affected by the development of atoll texture, and thus garnet may not be in equilibrium with the groundmass biotite [16].

Plagioclase crystals are also generally zoned. They consist of a relatively homogeneous, calcic core surrounded by a sodic rim (Fig. 4).

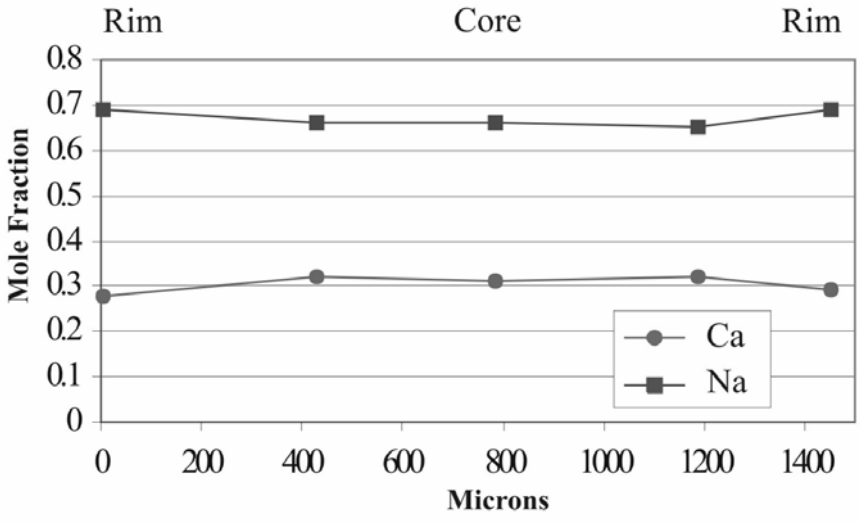

Fig. 4. Plagioclase zoning profile (sample 48), Note the increase of albite content in the rim of plagioclase crystal about the core

The calculation of cation formula units from the oxide weight percentages of mineral chemical analyses was carried out using version 0.92 of Program Mintab and the results are shown in Tables 1, 2 and 3.

Table 1. Electron-microprobe analyses of garnet from Ardara aureole samples

	76			73			48		
	Core	Near the rim	Rim	Core	Near the rim	Rim	Core	Near the rim	Rim
SiO_2	38.46	38.13	37.74	38.34	38.41	38.15	37.02	37.91	37.9
Al_2O_3	20.81	21.23	20.68	21.01	20.96	20.83	20.55	20.92	20.69
MgO	2.48	3.05	2.4	1.72	3.43	2.18	2.09	2.61	2.48
FeO	34.57	37.12	37.54	31	36.96	39.39	33.42	32.36	32.75
MnO	0.86	1.03	1.11	1.87	0.58	0.63	5.26	4.63	4.5
CaO	4.4	1.58	1.36	7.86	1.48	1.03	2.25	2.48	2.77
Total	101.58	102.14	100.83	101.8	101.82	102.21	100.59	100.91	101.09
Formula basis: 12 oxygens									
Si	3.041	3.011	3.031	3.019	3.033	3.033	2.986	3.026	3.027
Al	1.939	1.976	1.958	1.95	1.951	1.952	1.954	1.968	1.948
Mg	0.292	0.359	0.287	0.202	0.404	0.258	0.251	0.311	0.295
Fe	2.286	2.449	2.521	2.029	2.441	2.619	2.181	2.16	2.188
Mn	0.058	0.069	0.076	0.125	0.039	0.042	0.359	0.313	0.304
Ca	0.373	0.134	0.117	0.663	0.125	0.088	0.194	0.212	0.237
Total	7.989	7.998	7.99	7.988	7.993	7.992	7.925	7.99	7.999
X_{Al}	0.76	0.813	0.84	0.672	0.811	0.871	0.731	0.721	0.724
X_{Py}	0.097	0.119	0.096	0.067	0.134	0.086	0.084	0.104	0.098
X_{Gr}	0.124	0.045	0.039	0.22	0.042	0.029	0.065	0.071	0.078
X_{Sp}	0.019	0.023	0.025	0.041	0.013	0.014	0.12	0.104	0.101

	7			82	81	53	36
	Core	Near the rim	Rim	Near the rim	Near the rim	Near the rim	Near the rim
SiO_2	39.05	39.02	38.02	37.09	37.86	38.16	37.66
Al_2O_3	21.04	21.7	21	20.94	21.86	20.78	21.27
MgO	0.91	1.79	1.47	3.66	3.29	2.75	2.4
FeO	28.11	32.04	29.65	36.77	34.31	30.25	32.53
MnO	5.2	0.51	4.74	1.24	1.16	6.03	5.41
CaO	8.26	8.41	4.68	1.23	1.01	2.68	2.1
Total	102.57	103.47	99.56	100.93	99.49	100.65	101.37
Formula basis: 12 oxygens							
Si	3.054	3.015	3.058	3.042	3.059	3.044	3.002
Al	1.94	1.976	1.991	1.968	1.991	1.954	1.998
Mg	0.106	0.206	0.176	0.435	0.41	0.327	0.285
Fe	1.839	2.07	1.995	2.333	2.286	2.018	2.169
Mn	0.343	0.033	0.323	0.084	0.085	0.407	0.365
Ca	0.692	0.696	0.403	0.105	0.098	0.229	0.179
Total	7.974	7.996	7.946	7.967	7.929	7.979	7.998
X_{Al}	0.617	0.689	0.689	0.789	0.794	0.677	0.723
X_{Py}	0.036	0.069	0.061	0.147	0.142	0.11	0.095
X_{Gr}	0.232	0.232	0.139	0.036	0.034	0.077	0.06
X_{Sp}	0.115	0.011	0.111	0.028	0.03	0.137	0.122

Table 2. Electron-microprobe analyses of biotite from Ardara aureole samples

	76	73	48	7	82	81	53	36
SiO_2	34.99	37.95	36.7	36.9	35.407	34.98	36.96	36.56
Al_2O_3	24.08	20.93	19.74	19.33	20.192	20.63	20.04	19.71
TiO_2	1.91	2	1.79	1.76	1.35	2.29	1.65	1.87
MgO	7.06	8.83	10.19	10.59	9.494	9.12	10.3	9.81
FeO	18.21	19.6	17.75	17.61	19.115	19.33	17.79	18
MnO	0	0	0	0	0	0	0	0
CaO	0	0	0	0	0	0.19	0	0
Na_2O	0.36	0	0.37	0	0.573	0.64	0.26	0
K_2O	7.14	8.89	8.99	8.38	7.988	7.3	8.64	8.57
Total	95.28	98.2	95.53	94.57	94.119	94.48	95.64	94.52
Formula basis: 22 oxygens								
Si	5.185	5.51	5.49	5.542	5.397	5.303	5.5	5.512
^{IV}Al	2.815	2.49	2.51	2.420	2.603	2.697	2.5	2.488
^{VI}Al	1.518	1.09	0.97	1.002	1.024	0.989	1.015	1.014
Ti	0.213	0.22	0.2	0.199	0.155	0.261	0.185	0.212
Mg	1.679	1.91	2.27	2.371	2.156	2.061	2.285	2.205
Fe	2.257	2.38	2.22	2.212	2.437	2.451	2.214	2.27
Mn	0	0	0	0	0	0	0	0
Total	5.667	5.6	5.66	5.686	5.772	5.762	5.699	5.701
Ca	0	0	0	0	0	0.031	0	0
Na	0.181	0	0.11	0	0.168	0.188	0.075	0
K	1.35	1.67	1.72	1.621	1.554	1.412	1.64	1.648
Total	1.531	1.67	1.83	1.606	1.722	1.631	1.715	1.648
X_{Ph}	0.296	0.341	0.401	0.409	0.374	0.358	0.401	0.387
X_{ann}	0.398	0.425	0.392	0.384	0.422	0.425	0.388	0.398

Table 3. Electron-microprobe analyses of plagioclase from Ardara aureole samples

	76		73		48		7	
	Rim	Core	Rim	Core	Rim	Core	Rim	Core
SiO_2	58.96	57.55	63.43	60.46	61.86	61.06	59.94	59.23
Al_2O_3	25.92	27	24	26.35	24.42	25.19	26.02	25.86
FeO	0	0	0.59	0	0.31	0	0.23	0.26
CaO	8.02	8.52	4.94	7.25	5.89	6.33	6.09	6.59
Na2O	6.97	6.35	8.69	7.22	8.01	7.64	7.47	7.25
K2O	0	0	0	0	0	0	0	0
Total	99.87	99.42	101.65	101.28	100.49	100.22	99.75	99.19
Formula basis: 8 oxygens								
Si	2.63	2.59	2.77	2.66	2.73	2.7	2.66	2.651
Al	1.36	1.43	1.24	1.36	1.27	1.31	1.361	1.364
Fe	0	0	0.02	0	0.01	0	0.009	0.01
Ca	0.38	0.41	0.23	0.34	0.28	0.3	0.29	0.316
Na	0.6	0.55	0.74	0.61	0.69	0.65	0.643	0.629
K	0	0	0	0	0	0	0	0
X_{An}	0.388	0.427	0.237	0.358	0.289	0.316	0.311	0.334
X_{Ab}	0.612	0.573	0.763	0.642	0.711	0.684	0.689	0.666
	82		81		53		36	
	Rim	Core	Rim	Core	Rim	Core	Rim	Core
SiO_2	60.69	59.85	61.98	58.57	63.67	64.39	61.27	60.45
Al_2O_3	24.56	24.45	25.06	26.84	23.94	24.77	25.45	27.53
FeO	0	0	0	0	0.22	0	0	0

Table 3. Continued

CaO	5.94	6.32	5.93	8.44	8.73	8.09	7.58	6.78
Na2O	8.41	8.19	8.57	7.06	4.9	5.78	6.62	8.66
K2O	0	0	0	0	0	0	0	0
Total	99.6	98.81	101.54	100.91	101.46	103.03	100.92	103.42
Formula basis: 8 oxygens								
Si	2.708	2.695	2.71	2.6	2.78	2.76	2.694	2.608
Al	1.291	1.298	1.29	1.4	1.23	1.25	1.319	1.4
Fe	0	0	0	0	0.01	0	0	0
Ca	0.284	0.305	0.28	0.4	0.23	0.27	0.312	0.4
Na	0.727	7.15	0.73	0.61	0.74	0.67	0.646	0.567
K	0	0	0	0	0	0	0	0
X_{An}	0.281	0.041	0.277	0.396	0.237	0.287	0.326	0.414
X_{Ab}	0.719	0.959	0.723	0.604	0.763	0.713	0.674	0.586

a) Garnet-biotite geothermometry

In this study ten different calibrations of garnet-biotite thermometry were employed using version 2.1 of the program Thermobarometry of Kohn and Spear. To achieve temperature estimates from different calibrations it is necessary to have at least a rough idea of the pressure because the geothermometers are slightly pressure sensitive. Using petrogenetic grid constraints on aluminium-silicate assemblages, Naggar and Atherton [8] suggested that the Ardara aureole crystallized around 4.5 kbar, whilst Kerrick [13] suggested a pressure of 2.5 ± 0.5 kbar based on the Ghent et al. [17] calibration of the garnet-plagioclase-Al_2SiO_5-quartz geobarometery. As the Ardara aureole contains thermal kyanite, andalusite and sillimanite, the pressure at the peak of thermal metamorphism must have been slightly less than that of the aluminosilicate triple point. Therefore, using the aluminosilicate triple point from Pattison [18], 4 kbar seems a sensible estimate for pressure. The exact value is not critical, since changing the assumed pressure by 1 kbar only results in a 10 °C change in the estimated temperature.

Different calibrations for each sample produce the large diversity of temperature estimates (Fig. 5) and so it is worth discussing briefly the possible source of variation.

Firstly, compositional zoning in the garnet crystals produces diversity of temperature estimates. For samples in which garnets are zoned estimated temperatures were calculated using:
pairs of garnet core analyses and matrix biotite composition
pairs of the near-rim of garnet analyses and matrix biotite composition and
pairs of garnet rim analyses and matrix biotite composition

The lowest temperature estimates are generally from the outermost rim of garnet analyses coupled with the matrix biotite composition (Fig. 5). The reverse zoning in the outermost rims of garnet probably formed due to retrograde reaction [16] and temperature estimates from the outermost rims of the garnet analyses together with matrix biotite, and are therefore not representative of peak metamorphic conditions. In contrast, the near-rim analyses of garnet, together with matrix biotite compositions usually produce the highest estimates of temperature, probably indicating peak metamorphic conditions (Fig. 5).

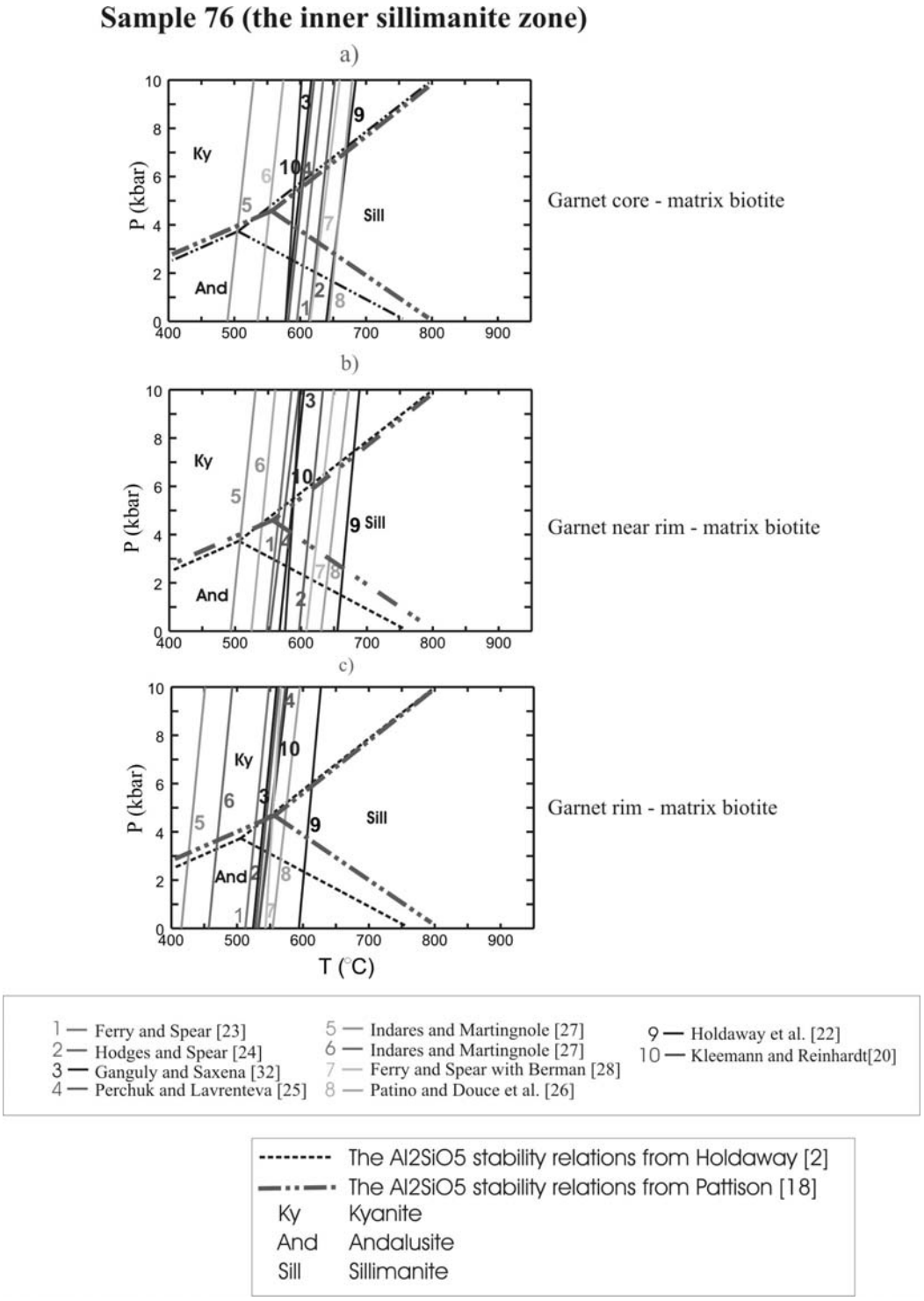

Fig. 5. P-T diagram showing results from the ten different calibrations of garnet-biotite thermometry of sample 76 from:
a) pairs of garnet core analyses and matrix biotite composition,
b) pairs of the near-rim of garnet analyses and matrix biotite composition and
c) pairs of garnet rim analyses and matrix biotite composition

Garnet core analyses, together with matrix biotite composition, generally provide lower temperature estimates than those from pairs of the near-rim of garnet analyses and matrix biotite composition, and higher temperature estimates than those from pairs of the outermost rim of garnet analyses and matrix biotite composition (Fig. 5). As the temperatures derived from garnet core compositions coupled with matrix biotite compositions lack geologic significance [19], the near-rim analyses of garnet together with matrix biotite compositions are likely to give more reliable geothermometric results

Secondly, the different calibrations will necessarily lead to different estimates of temperature because they utilize different activity models for garnet and biotite. The temperature estimates produced from ten different calibrations of a garnet-biotite geothermometer using the near-rim analyses of garnet together with matrix biotite composition for analysed samples are given in Table 4.

Table 4. Temperature estimates produced from ten different calibrations of garnet-biotite geothermometer using the near-rim analyses of garnet together with matrix biotite composition with nominal P of 4 kb for eight analysed samples from the Ardara aureole

Sample Calibration	82	81	76	73	53	48	36	7
Ferry and Spear [23]	636.4	633.1	580.9	628	537.7	502.6	491.4	401.5
Hodges and Spear [24]	651	645.9	622.9	645	564.7	529.8	514.3	481.6
Perchuk and Lavrent'eva [25]	582	586.4	590.7	589.1	545.9	515.9	515	454.5
Ganguly and Saxena [32]	609.5	607.9	580.2	605.2	554.5	535.8	529.1	472.4
Indares and Martignole [27]	573.8	540.2	516.2	534.4	556.6	500.7	488.6	435.7
Indares and Martignole [27]	594.8	563.9	548.7	570.1	508.1	472.4	454.8	437.2
Ferry and Spear with Berman [28]	648.2	643.3	634.9	646.8	563.9	531.6	515.1	486.3
Patino Douce et al. [26]	663.6	644.1	658.1	656.2	573.8	538.3	521.7	494.8
Holdaway et al. [22]	676.1	668.6	671.6	669.6	645	616.6	605.1	599.9
Kleemann and Reinhardt [20]	603.6	598.2	589.2	598.9	561.3	543.6	534.5	517.5

Which calibration gives the most precise and accurate result? It is impossible to say because there is not yet a general agreement on this aspect [20, 21]. Unfortunately most authors do not state why they choose the calibration they use (for example see Kerrick, [13]). In addition, there are numerous examples where the preferred or chosen garnet-biotite calibration was the one that fitted other temperature data best [20]. Therefore, it is very difficult to choose a garnet-biotite calibration as the most accurate and reliable one for this study.

Holdaway et al. [22] provides the most recent calibration of garnet-biotite geothermometry. However in the present study, the Holdaway et al. [22] calibration gives very high temperatures which seem suspect, especially for andalusite-bearing rocks.

Kleemann and Reinhardt [20] tested eleven published versions of the garnet-biotite thermometer (e.g. Ferry and Spear, [23]; Hodges and Spear, [24]; Perchuk and Lavrent'eva, [25]; Patino Douce et al. [26]; Indares and Martignole, [27]) by applying them to the experimental data of Ferry and Spear [23] and Perchuk and Lavrent'eva [25]. Their statistical evaluation demonstrated that most calibrations published to date could not be applied for general use. However, on the basis of statistical data they found that their own calibration had the highest accuracy compared with the other eleven calibrations. In addition, Kleemann and Reinhardt [20] used the garnet activity model of Berman [28], which according to Spear [21] best reproduced the available experimental data at that time. Therefore, for the purpose of thermometry in this study the author preferred to use the Kleemann and Reinhardt [20] calibration. This calibration gives temperatures of approximately 510 to 605 ºC across the Ardara

aureole (Fig. 6). Considering the error on the calibration (± 50 ºC) and the other problems mentioned above, the quoted temperature estimates are possibly only sensibly accurate to ± 75 ºC.

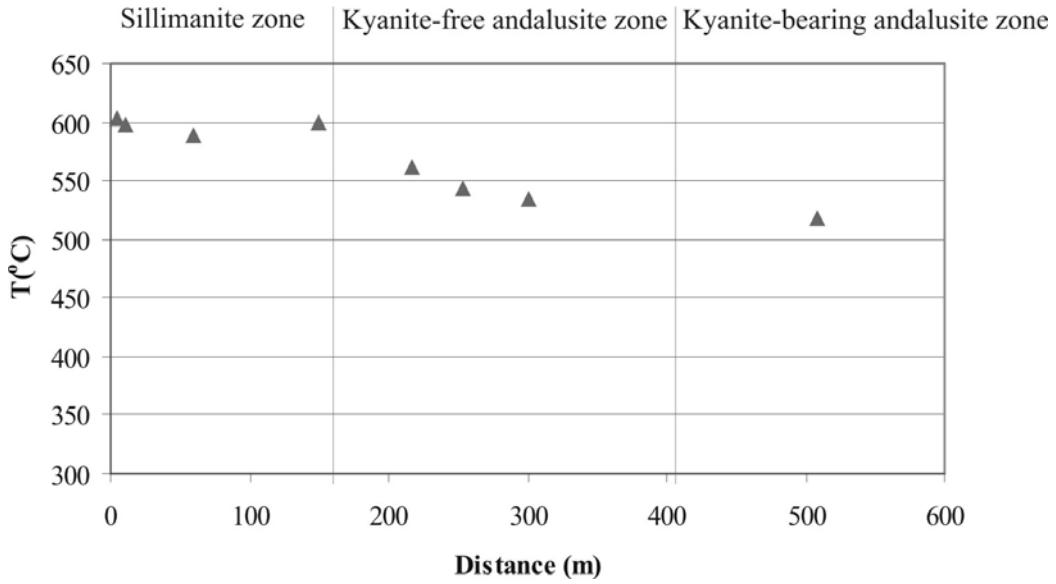

Fig. 6. Plot of temperature as function of distance from the contact of the Ardara pluton, Temperatures for the data points were derived using the Kleemann and Reinhardt [20] calibration of garnet-biotite geothermometer

b) Garnet-plagioclase-Al_2SiO_5-quartz geobarometry

In the following study, five calibrations of garnet-plagioclase-Al_2SiO_5-quartz (GASP) barometry are employed using version 2.1 of the program Thermobarometry of Kohn and Spear.

To obtain estimates of pressure it is necessary to have at least a rough idea of the temperature because the geobarometers are slightly temperature sensitive. The temperature estimates from Kleemann and Reinhardt's [20] calibration have been used in this study.

The range of pressure estimates using the different calibrations for GASP barometry is quite large (Fig. 7). The spread of pressure estimates is partly due to the presence of chemical zoning in garnet and plagioclase crystals. For samples in which garnets and plagioclase are zoned, estimated temperatures were calculated using:

pairs of garnet core analyses and plagioclase core composition

pairs of garnet core analyses and plagioclase rim composition

pairs of the near-rim of garnet analyses and plagioclase core composition and

pairs of the near-rim of garnet analyses and plagioclase rim composition

For samples in which only plagioclase is zoned, estimated temperatures were calculated using:

pairs of the near-rim of garnet analyses and plagioclase core composition and

pairs of the near-rim of garnet analyses and plagioclase rim composition.

The sodic rim of plagioclase crystals together with the calcic core of garnet grains produced the highest pressure estimates (Fig. 7). The pressure estimates from garnet core analyses together with the calcic core of plagioclase are also quite high (Fig. 7). Since pressure estimates from garnet core analyses together with either the sodic rim and calcic core of plagioclase are well above the stability limit of andalusite, these results seem suspect and are not used in this study. On the other hand, the lowest pressure estimates come from the calcic core of zoned plagioclase together with the near-rim

composition of garnet crystals (Fig. 7). The pressure estimates from the near-rim of garnet analyses coupled with the sodic rim of plagioclase give higher pressure (approximately 1 kbar) than pairs of the near-rim of garnet composition and calcic core of plagioclase (Fig. 7). As mentioned earlier, the author believes that the outermost rims of garnet which show the reverse zoning profile probably formed due to retrograde reaction and so the analyses from outermost rims of garnet were not used for the purpose of barometry.

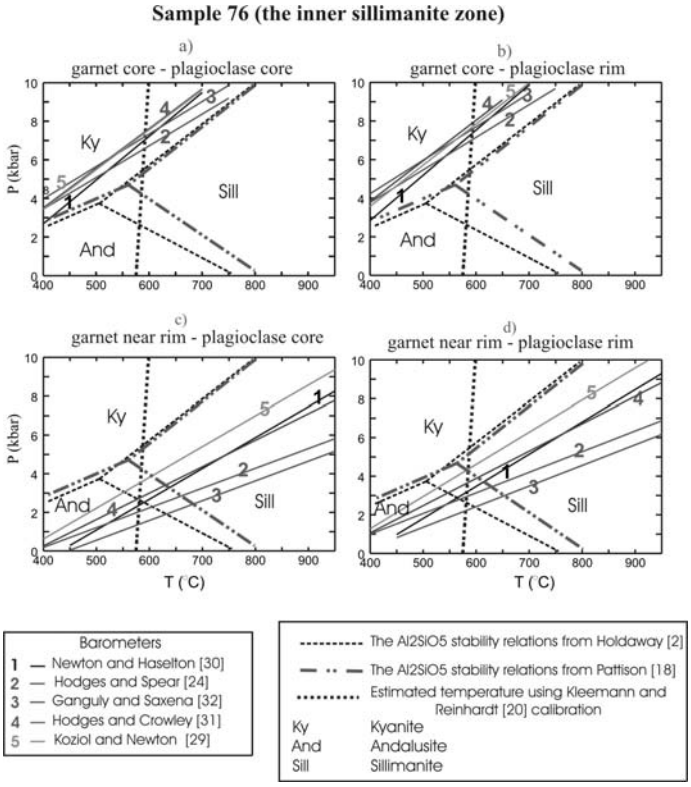

Fig. 7. P-T diagram showing results from the five different calibrations of GASP barometry of sample 76 from:
a) pairs of garnet core analyses and plagioclase core composition
b) pairs of garnet core analyses and plagioclase rim composition
c) pairs of the near-rim of garnet analyses and plagioclase core composition and
d) pairs of the near-rim of garnet analyses and plagioclase rim composition

The sodic rim of plagioclase probably formed due to retrograde reaction [9], and so it seems that the near-rim of garnet analyses coupled with calcic core composition of plagioclase are most likely to represent peak equilibrium conditions and thus provide the most accurate pressure estimates for this study.

Part of the spread of pressure estimates also comes from using different calibrations for GASP barometry. The pressure estimates produced from five different calibrations of GASP barometry using the near-rim analyses of garnet together with plagioclase core composition for analysed samples are given in Table 5. The Koziol and Newton [29] calibration generally gives the highest overall pressure, which is approximately 1 kbar higher than the other calibrations. However, at the higher grossular contents, it tends to converge with the Hodges and Spear [24], Newton and Haselton [30] and Hodges and Crowley [31] calibrations because the Koziol and Newton [29] calibration results in the highest activity for grossular.

Table 5. Pressure estimates produced from five different calibrations of GASP barometry using the near-rim analyses of garnet together with plagioclase core composition for eight analysed samples from the Ardara aureole, The nominal T used by the Kleemann and Reinhardt [20] calibration

Sample Calibration	82	81	76	73	53	48	36	7
Newton and Haselton [30]	3.1	1.5	2.3	3.05	2.9	3.8	3.2	8.4
Hodges and Spear [24]	2.9	1.15	2	2.8	3.15	3.9	3.2	8.8
Ganguly and Saxena [32]	2.15	0.4	1.3	2.05	2.05	3.15	2.8	11.5
Hodges and Crowley [31]	3.95	2.05	2.8	3.7	3.9	4-2	3.9	9.9
Koziol and Newton [29]	4.7	2.95	3.8	4.3	3.45	3.9	3.8	8.38

The Ganguly and Saxena [32] calibration provides a lower pressure (approximately 1 kbar) than the rest of the calibrations at low grossular contents. It also tends to provide similar results with the rest of the calibrations at higher grossular contents because this calibration results in the lowest activity for grossular.

As the Koziol and Newton [29] calibration uses the most recent and best reversed experimental data [21] it seems reasonable to apply this calibration for the estimation of the pressure of the Ardara aureole. As it can be seen in Table 5, the pressure estimate from sample 7 is quite high and lies well beyond the stability field of andalusite, suggesting most probably disequilibrium. The high pressure calculated from sample 7 seems inappropriate in this case. Ignoring sample 7, the total range of pressure estimates is between 2.95 and 4.7 kbar. Considering average pressure estimates calculated from different samples, a value of around 4 kbar seems sensible for the best estimate of pressure at the thermal metamorphic peak in this area.

Considering the range of pressure estimates produced from different samples and the errors of ± 0.5 kbar on the calibration itself, the net uncertainty in this pressure estimate must be of the order of ± 1 kbar.

c) Discussing the results

Using the Kleemann and Reinhardt [20] calibration of garnet-biotite geothermometry and the Koziol and Newton [29] calibration of GASP barometry, temperature estimates for eight analysed samples from the Ardara aureole are plotted along with the three univariant reactions of the Al_2SiO_5 triple point of Richardson et al. [33] and Pattison [18], as well as andalusite=sillimanite curves of Holdaway [2] (Fig. 8). As can be seen in Fig. 8 the calculated temperatures for analysed samples are in very good agreement with the andalusite=sillimanite equilibrium determined by Pattison [18] at 4 kbar, but not with those from Richardson et al. [33] and Holdaway [2]. The position of the andalusite=sillimanite equilibrium has long been an enigma. The two most widely cited experimental determinations of andalusite=sillimanite are those of Richardson et al. [33] and Holdaway [2]. Pattison and Tracy [3] provide the most recent review of experimental determinations of the andalusite=sillimanite equilibrium. They questioned the andalusite=sillimanite curve of Richardson et al. [33] due to the problems of ultra-grinding and the presence of fibrolite in their experiments. However, Pattison and Tracy [3, p 167] stated:

" Nevertheless, the Holdaway [2] andalusite=sillimanite curve is not without its critics, typically petrologists who find apparent petrologic inconsistencies in natural assemblages when the restricted andalusite stability field of Holdaway [2] is combined with other existing experimental and phase equilibria constraints. These include: the occurrence of andalusite in granites and migmatites; widespread occurrence of muscovite-cordierite-andalusite-quartz±chlorite assemblages [18]".

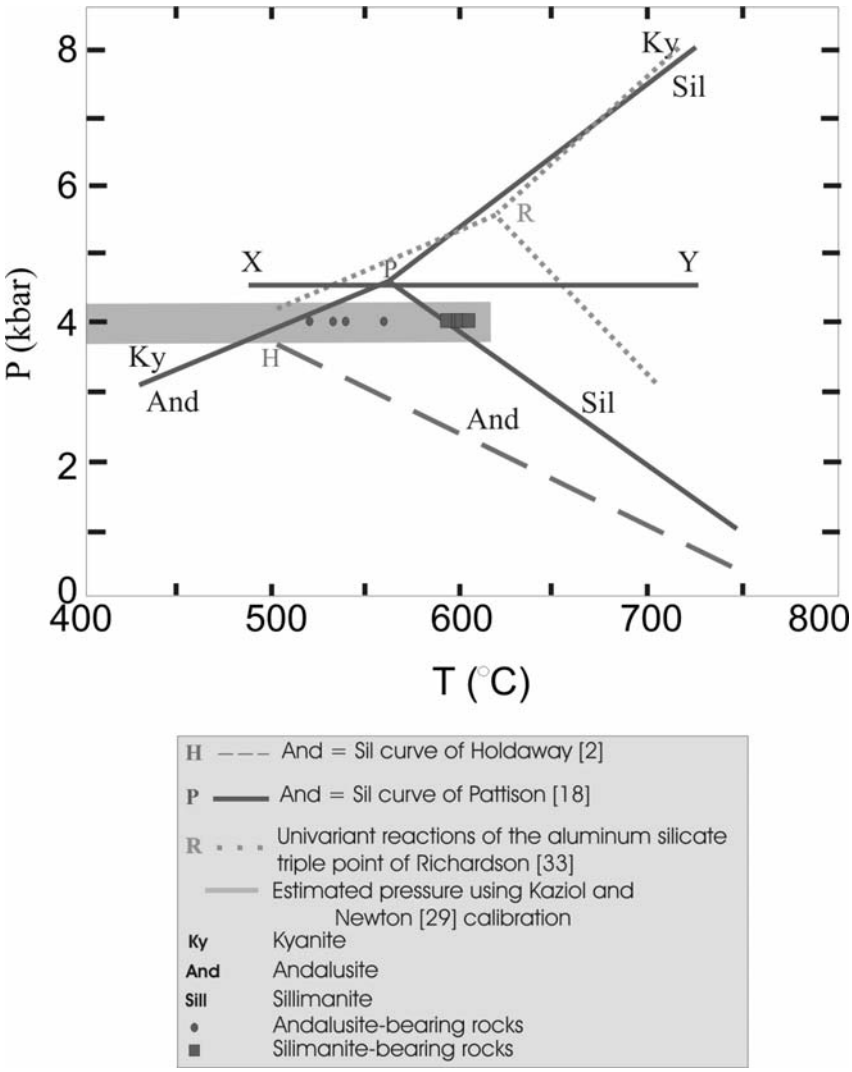

Fig. 8. P-T diagram showing temperature estimates produced from Kleemann and Reinhardt [20] calibration of garnet-biotite thermometery considering P=4 kbar from eight samples from the Ardara aureole, XY shows possible crystallization path in the Donegal aureoles according to Naggar and Atherton [8]

Pattison [18] determined the andalusite=sillimanite curve on the basis of the first appearance of sillimanite at, or immediately upgrade of, the muscovite + quartz=andalusite + Kfeldspar in the Ballachulish aureole, Scotland. According to Pattison and Tracy [3] the andalusite=sillimanite curve of Pattison [18] satisfies most of the petrological arguments used to support either the Richardson et al. [33] or Holdaway [2] curves. Therefore, it seem reasonable to use Pattison's [18] andalusite=sillimanite determination rather than that of Holdaway [2].

Acknowledgments- I would like to express my sincere gratitude to Dr. A. P. Boyle, and Dr. M. P. Atherton from the University of Liverpool for their considerable efforts, support and guidance. The author should also thank Mr. Case Veltkempt for help with SEM work at Liverpool.

REFERENCES

1. Kerrick, D. M. (1990). The Al_2SiO_5 polymorphs, *Reviews in Mineralogy, 22*, 406.
2. Holdaway, M. J. (1971). Stability of andalusite and the aluminium silicate phase diagram, *American Journal of Science, 271*, 97-131.
3. Pattison, D. R. M. & Tracy, R. J. (1991). Phase equilibria and thermobarometry of metapelites. In Reviews in Mineralogy, 26: Contact metamorphism (ed. D. M. Kerrick). *Mineralogical Society of America*, 105-206.
4. Pitcher, W. S. & Berger, A. R. (1972). *The geology of Donegal: A study of Granite Emplacement and Unroofing*. New York, John Wiley.
5. Akaad, M. K. (1956a). The Ardara granitic diapir of Co. Donegal, G*eological Society of London Quaternary Journal, 112*, 263-88.
6. Akaad, M. K. (1956b). The northern aureole of the Ardara pluton of County Donegal, *Geological Magazine, 93*, 377-92.
7. Pitcher, W. S. & Read, H. H. (1963). Contact metamorphism in relation to manner of emplacement of the granites of Donegal, *Journal of Geology, 71*, 261-96.
8. Naggar, M. H. & Atherton, M. P. (1970). The composition and metamorphic history of some aluminum silicate-bearing rocks from the aureoles of the Donegal granites, *Journal of Petrology, 11*, 549-589.
9. Homam, S. M. (2000). A chemical and textural study of aluminium silicate-bearing rocks from the contact aureole of the Ardara pluton. Co. Donegal, Ireland. Ph.D Thesis, University of Liverpool.
10. Vernon, R. H. & Paterson, S. R. (1993). The Ardara pluton, Ireland: deflating an expanded intrusion, *Lithos, 31*, 17-32.
11. Holder, M. T. (1979). *An emplacement mechanism for post-tectonic granites and its implications for their geochemical features*. In: Atherton, M. P. and Tarney, J. (ads.), Origin of Granite Batholiths. Geochemical Evidence, Shiva, Orpington.
12. Homam, S. M., Boyle, A. P. & Atherton, M. P. (2002). Syn-to post-kinematic fibrolite-biotite intergrowth in the Ardara aureole NW Ireland. *Journal of Sciences, Islamic Repoblic of Iran, 13*, 327-337.
13. Kerrick, D. M. (1987). Fibrolite in contact aureoles of Donegal, *American Mineralogist, 72*, 240-254.
14. Essene, E. J. (1989). *The current status of thermobarometry in metamorphic rocks*, In: Daly, J. F., Cliff, R. A. & Yardley, B. W. D. (eds) Evolution of metamorphic belts, Oxford, Blackwell scientific Publications.
15. Albee, A. L. & Ray, L. (1970). Correction factors for electron probe microanalysis of silicates, oxides, carbonates, phosphates and sulfates, *Analytical. Chemistry, 42*, 1408-1414.
16. Homam, S. M. (2003). Formation of atoll garnets in the Ardara aureole, N W Ireland. *Journal of Sciences, Islamic Repoblic of Iran, 14*, 247-258.
17. Ghent, E. D., Robbins, D. B. & Stout, M. Z. (1979). Geothermometry, geobarometry, and fluid compositions of metamorphosed calc-silicates and pelites, Mica Creek, *American Mineralogist, 66*, 702-722.
18. Pattison, D. R. M. (1992). Stability of andalusite and sillimanite and the Al_2SiO_5 triple point: Constraints from the Ballachullish aureole, *Scottish Journal of Geology, 100*, 423-446.
19. Spear, F. S. & Selverstone, J. (1983). Quantitative P-T paths from zoned minerals: Theory and tectonic applications, *Contributions to Mineralogy and Petrology, 83*, 348-357.
20. Kleemann, U. & Reinhardt, J. (1994). Garnet-biotite thermometry revisited: The effect of Al^{VI} and Ti in biotite, *European Journal of Mineralogy, 6*, 925-941.
21. Spear, F. S. (1995). *Metamorphic phase equilibria and pressure-temperature-time paths*, Washington, DC, Mineralogical Society of America Monograph.

22. Holdaway, M. J., Mukhopadhyay, B., Dyar, M. D., Guidotti, C. V. & Dutrow, B. L. (1997). Garnet-biotite thermometry revisited: New Margules parameters and a natural specimen data set for Maine, *American Mineralogist, 82*, 582-595.
23. Ferry, J. M. & Spear, F. S. (1978). Experimental calibration of the partitioning of Fe and Mg between biotite and garnet, *Contributions to Mineralogy and Petrology, 66*, 113-117.
24. Hodges, K. V. & Spear, F. S. (1982). Geothermometry, geobarometry and the Al_2SiO_5 triple point at Mt. Moosilauke, new Hampshire, *American Mineralogist, 67*, 1118-1134.
25. Perchuck, L. L. & Lavrent'eva, I. V. (1983). *Experimental investigation of exchange equilibria in the system cordierite-garnet-biotite. In: Saxena, S. K., (ed) Kinetics and equilibrium in mineral reaction*. New York, Springer Verlag.
26. Patino Douce, A. E., Johnston, A. D. & Rice, J. M. (1993). Octahedral excess mixing properties in biotite: A working model with applications to geobarometry and geothermometry, *American Mineralogist, 78*, 113-131.
27. Indares, J. & Martignole, J. (1985). Biotite-garnet geothermometry in the granulite facies: the influence of Ti and Al in biotite, *American Mineralogist, 70*, 272-278.
28. Berman, R. G. (1990). Mixing properties of Ca-Mg-Fe-Mn garnets, *American Mineralogist, 75*, 328-344.
29. Koziol, A. M. & Newton, R. C. (1988). Redetermination of the anorthite breakdown reaction and improvement of the plagioclase-garnet-Al_2SiO_5-quartz geobarometer, *American Mineralogist, 73*, 216-223.
30. Newton, R. C. & Haselton, H. T. (1981). *Thermodynamics of the plagioclase-garnet-Al_2SiO_5-quartz geobarometer. In: Newton, R. C. (ed) Thermodynamics of Minerals and Melts*. New York, Springer Verlag.
31. Hodges, K. V. & Crowley, P. D. (1985). Error estimation geothermobarometry for pelitic systems, *American Mineralogist, 70*, 702-709.
32. Ganguly, J. & Saxena, S. K. (1984). Mixing properties of aluminosilicate garnets: constrains from natural and experimental data, and applications to geothermo-barometry, *American Mineralogist, 69*, 88-97.
33. Richardson, S. W., Gilbert, M. C. & Bell, P. M. (1969). Experimental determination of kyanite-andalusite and andalusite-sillimanite equilibria: the aluminium silicate triple point, *American Journal of Science, 267*, 259-72.